PARASITE DRAG REDUCTION OF A TWIN ENGINE LIGHTWEIGHT HELICOPTER CONFIGURATION

R. Reß, M. Grawunder, C. Breitsamter,
Institute of Aerodynamics and Fluid Mechanics, Technische Universität München,
Boltzmannstr. 15, 85748 Garching, Germany

Abstract

The present paper summarizes results of a three year research effort in investigating and improving means of drag reduction for twin-engine lightweight helicopters. In the focus of the work is the parasite drag under the influence of a rotating five blade rotor head. The optimization process comprises consecutive wind tunnel campaigns and accompanying numerical studies related to landing gear modification, flow control at the aft-body, and mast fairing modifications. The resulting shape modifications and means of flow control provide a drag reduction of up to 23% with respect to the unmodified configuration.

Nomenclature

C_D	drag coefficient
C_L	lift coefficient
C_m	pitching moment coefficient
C_p	pressure coefficient
u	axial velocity component
U_∞	freestream velocity
Re	Reynolds number
M_a	Mach number
TEL	twin engine light
AOA, α	angle of attack
AOS, β	angle of sideslip
VG	vortex generator

INTRODUCTION

Fuel saving and the reduction of emissions form the key challenges for the future of aviation. To approach this issue, the European Union together with the European aeronautical industry launched the CleanSky–Initiative [1]. Within CleanSky's Green Rotorcraft Consortium 2, the subproject "ADHeRo" (**A**erodynamic **D**esign Optimization of a **He**licopter Fuselage Including a Rotating **Ro**tor Head) deals with the reduction of parasite drag of a twin engine lightweight helicopter fuselage. Helicopters of this class possess a maximum takeoff weight of about 3 tons. Considering the multiple tasks these helicopters have to fulfill [2] [3], the rear loading capability usually poses an additional requirement. Earlier investigations [4] already have demonstrated that rotor head, landing gear, and the fuselage form about 74% of the total parasite drag of such a helicopter. The emphasis of the ADHeRo project lies on shape optimization of these particular components through wind tunnel testing. The tests are accompanied by numerical analyses [5],[6]. During the initial phase, a baseline configuration is defined and a corresponding wind tunnel model is completed. In the course of the program, landing gear, flow control devices, and the rotor head including the mast fairing are to be improved with respect to their contribution to the total parasite drag.

1. GEOMETRY

As the ADHeRo project addresses drag reduction of twin engine lightweight helicopters with rear loading capability, the chosen model geometry closely resembles the production version of a typical helicopter of this class.

1.1. Baseline Configuration

Focusing on the mentioned components, and in order to clearly identify effects of the shape variations, a reduced geometry is defined as the baseline wind tunnel model. Fig 1 shows the baseline configuration model comprising cabin, skid landing gear, a truncated tailboom, and a powered 5-blade rotor head. The geometry features all important details of the rotor head, the bulged windows, door handle, and a long footstep at the skid landing gear.

Fig.1. Baseline configuration, TEL-class helicopter fuselage with rotating rotor head

A fundamental set of aerodynamic data is gathered with the baseline configuration, serving as a reference for the proposed shape modifications.

2. EXPERIMENTS AND NUMERICS

As mentioned above, the scope of the work covers shape modification through consecutive wind tunnel experiments, as well as complementary numerical analyses.

2.1. Wind Tunnel Testing

The wind tunnel experiments are conducted in the facilities of the Institute of Aerodynamics and Fluid Mechanics at the Technische Universität München. The selected wind tunnel A is a low speed closed-circuit type wind tunnel. It can be operated with a closed, or with an open test section. In the latter configuration, a maximum speed of about 65 m/s can be attained. The size of the test section measures 1.8 x 2.4 x 4.8 m³.

2.2. Model

For the wind tunnel tests, a 1:5 scale model of the chosen helicopter configuration is designed, including all the components, which are subject to the envisaged shape modifications and aerodynamic investigations.

Fig.2. Modular design of the wind tunnel model

Fig.2 shows the modular structure of the 1:5 scale wind tunnel model, allowing for an easy change of components during the test runs. The model is equipped with a removable electrically powered rotor head. The rotor blades are truncated at the radial position of the first effective aerodynamic blade section. Provision is made for cyclic and collective pitch variation (see Figures 3 and 4).

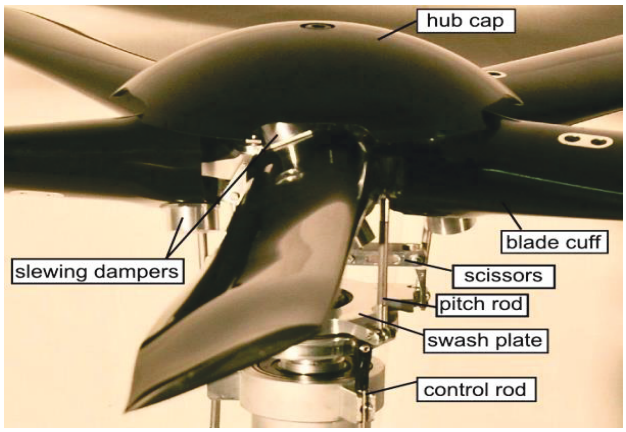

Fig.3. Model rotor head

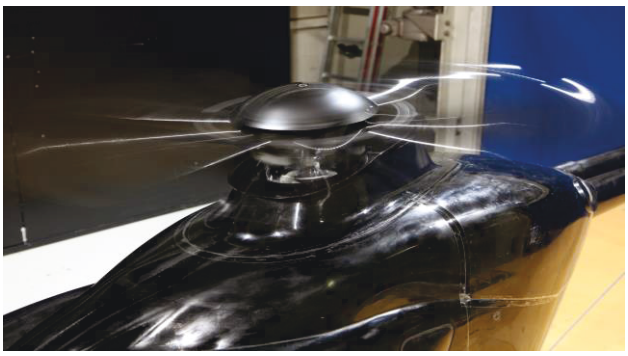

Fig.4. Rotating model rotor head

In order to facilitate surface pressure measurements, the model possesses 218 pressure taps. The majority of the taps are positioned around the aft-body, where drag reducing measures can be examined effectively. For a detailed description of the model design see [7].

2.3. Measurement Equipment

The measurement of aerodynamic forces and moments is carried out using a six component underfloor balance. The model's tailboom is connected to the balance via a horizontal sting and a vertical strut. The rotatable balance and an additional step motor drive for rotational movements of the model allow for adjusting AOA and AOS. For the ADHeRo project the polar definitions require a variation of AOA and AOS within the range of -10° to +10°.

For measuring steady surface pressures, 192 of the pressure taps are connected via tubes to three 64-channel pressure scanners. The remaining 26 taps are equipped with transient pressure sensors, mounted near the model surface. The pressure scanners are installed inside the model. The pressure and force measurements are averaged over 15 seconds per measurement point. Unsteady pressure data are sampled at a rate of 4 kHz and filtered with a 1 kHz low pass filter.

The flowfield measurements in the wake of the fuselage are conducted by means of a stereo particle-image-velocimetry (PIV) system with a laser pulse repetition rate of 10Hz (see Fig 5).

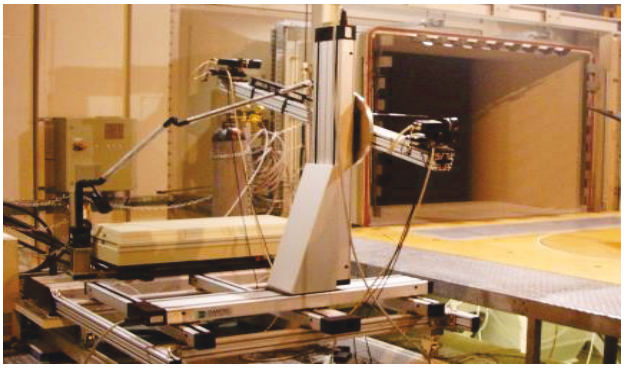

Fig.5. Stereo PIV system

Concerning the helicopter model, the rotor head settings for the wind tunnel experiments correspond to

the conditions of a trimmed fast forward flight. During the polar runs, the initial cyclic and collective pitch settings remain unchanged. Neither flapping nor lead–lag movements of the rotor blades are reproduced. The rotational speed of the rotor head is set to 963 rpm. The wind tunnel experiments are carried out at a freestream velocity of 40 m/s, yielding a Reynolds number of about $1x10^6$.

2.4. Numerical Method

The numerical simulations are performed for selected configurations. Flow modelling is based on the incompressible (Unsteady) Reynolds Averaged Navier-Stokes ((U)RANS) equations employing the commercial flow solver ANSYS CFX5 [8]. The mesh generation is carried out with the meshing tool ANSYS ICEM CFD. The computational domain is depicted in Fig. 6. It consists of an outer box with farfield dimensions of 10 times the reference length in streamwise direction $l_{x,ref}$. An inner domain is used for the rotor head to apply the sliding mesh technique for the rotor head rotation and dynamic mesh movement for the cyclic pitch [9]. Unstructured meshes are employed using the Octree method first to obtain the surface grids. Several smoothing loops are attributed to the surface grids before the volume mesh is set up with the Delauney algorithm. The obtained volume mesh is smoothed again before adding the prism layers. The prism layers, consisting of 24 single layers, are generated near the solid walls. The equivalent dimensionless wall distance y+ is confined below one on all no-slip surfaces. Fig. 7 presents a typical mesh for the baseline configuration. For the wake region, the grid is refined to ensure a sufficient spatial resolution for the wake vortical structures progressing downstream. The computations are carried out employing the standard Shear Stress Transport (SST) turbulence model. For the spatial discretization, a High Resolution Scheme is employed, blending between first and second-order accuracy. The temporal discretization is realized through the application of the implicit Backward Euler Method with second-order accuracy. All simulations are carried out using a physical timescale of 1×10^{-4} s. The boundary conditions for the simulations are defined by the inflow with a constant velocity profile at the inlet (turbulence intensity of 5%), the outflow with zero pressure gradient at the outlet, no-slip walls at the surface of the model and free-slip walls at the side-walls, the top, and the bottom of the domain.

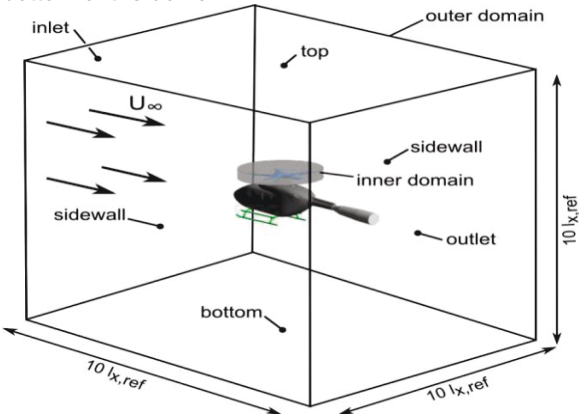

Fig.6. Computational domain.

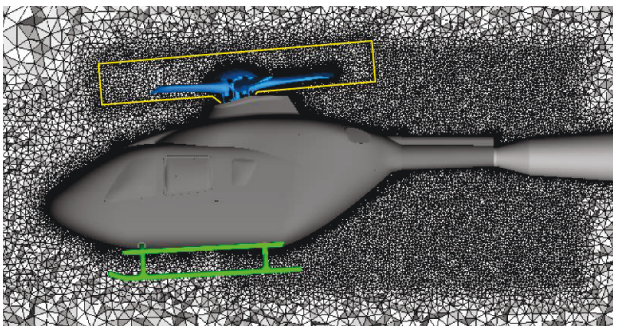

Fig.7. Unstructured mesh for the baseline configuration (rotor head domain interface indicated by yellow box).

3. RESULTS AND DISCUSSION

Experimental and numerical data representing the major modification steps within ADHeRo are analyzed with a focus on the effects of the shape modifications on the flowfield around the aft-body. In this zone, the most significant changes of the flow topology coinciding with drag reduction are expected.

The presented aerodynamic force and moment coefficients (see sections 3.2-3.4) always refer to the total drag, total lift, and total pitching moment of the particular configuration and are taken from results of the force and moment measurements. Unless otherwise noted, the presented experimental data are taken from measurements with the full configuration including rotor head and the specified components. These are either the baseline or modified instances.

3.1. Baseline Configuration

During the baseline wind tunnel campaign, a comprehensive data set comprising aerodynamic forces and moments, surface pressure, and flowfield data in the wake of the model is established. In order to identify the individual contributions of single components to the total drag, several configurations omitting the rotor head, the skid landing gear, or even both are investigated. The data set of the baseline campaign is used for comparisons with data obtained with the modified geometries. The first of the modification steps concerns the skid landing gear. During the subsequent phases of ADHeRo, flow control measures at the aft-body, the modification of the mast fairing and the rotor hub are examined.

3.2. Skid Landing Gear Modification

In order to reduce flow separation at the cross beams without impairing the flowfield around the aft-body, two modified skid landing gears (designated L1 and L2) are investigated. For comparison, Fig.8 shows the baseline skid landing gear variant with the baseline underbody. Fig.9 shows the variant L1, designed to be easily retrofitted to the production helicopter, while variant L2 (depicted in Fig.10) forms a more progressive variant, necessitating a redesign of structural elements of the helicopter fuselage. Both skid landing gear modifications are combined with an aerodynamically refined underbody. The design process for the optimized skid landing gear variants is described in detail in [5]. The modified variants feature faired

crossbeams and faired attaching elements. The fairings are designed according to the airfoil geometry specification DU-06-W200. For compliance with crash worthiness constraints, the thickness of the airfoil section is chosen in a way that it encloses the cross beam with sufficient offset to the tube. For the progressive variant L2, the attaching elements of the crossbeams are relocated into the fuselage, offering a decrease in frontal area in addition to an aerodynamically clean underbody.

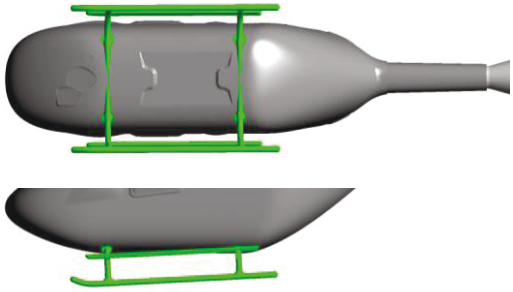

Fig.8. Baseline skid landing gear L0

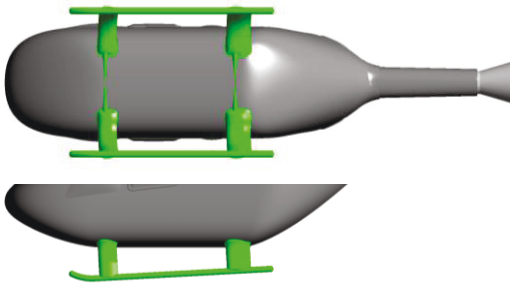

Fig.9. Modified skid landing gear L1

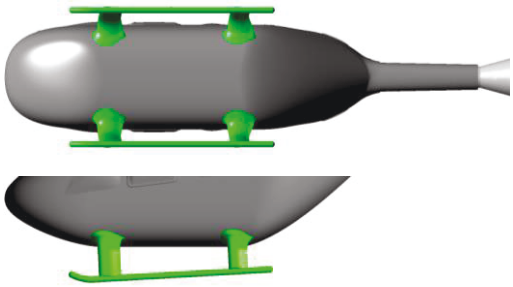

Fig.10. Modified skid landing gear L2

First, the effectiveness of the shape modifications is analyzed using the flowfield data generated through PIV measurements. Fig.11 shows the mean axial velocity component of the flowfield in the indicated cross flow plane downstream of the investigated skid landing gears. The presented velocity data are normalized with the freestream velocity U_∞. For the baseline configuration (Fig.11 top), the deficit in mean axial velocity caused by the flow separation at the fuselage upsweep is clearly visible in the backdoor center area. The mean axial velocity is decreased over a wide spatial range by 40% to 50%. Also, in the wake of the cylindrical beams of the baseline skid landing gear a significant axial velocity deficit can be detected. These large areas of decreased axial velocity coincide with high form and interference drag of the baseline skid landing gear configuration. The aerodynamic efficiency of the airfoil-shaped fairings at the modified skid landing gears becomes obvious in Fig.11 (bottom left and right). Apparently, the configurations with faired skid landing gears generate distinctively smaller areas of retarded axial flow with reduced maximum deficit levels.

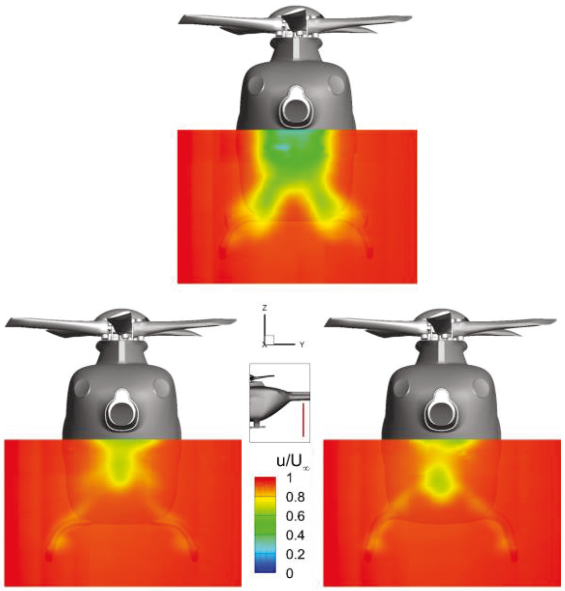

Fig.11. Mean axial velocity distribution: u/U_∞, α, β= 0°, baseline (top), L1 (bottom left), and L2 (bottom right), Re = 1 x 10^6

The velocity deficit associated with the wake of the faired skid landing gears itself is hardly detectable. For the baseline skid landing gear, this wake shows a velocity deficit of approximately 40%, while for the faired skid landing gears a thin sheet of velocity deficits of only 10 % is present. The progressive L2 variant differs from L1 in creating an area with high velocity deficit separated into two parts by an area without significant velocity deficit. It is obvious, that both modifications alleviate flow separation and significantly reduce the velocity deficit in the wake downstream of the backdoor region (see [5]). As a result, considerably lower drag coefficients for the streamlined skid landing gear configurations can be expected.

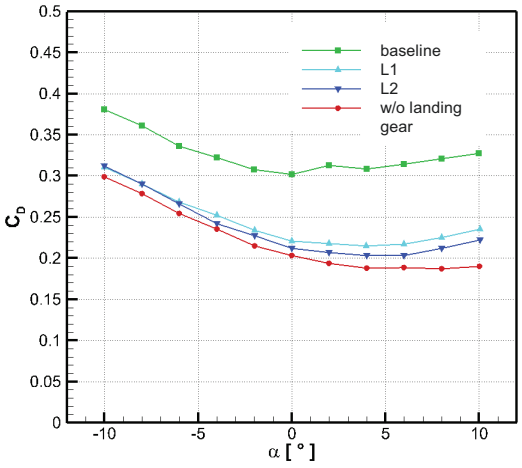

Fig.12. Drag coefficient vs AOA, AOS = 0°, Re = 1x10^6

Fig.12 shows the drag coefficient as function of AOA for the baseline configuration and the modified configurations with skid landing gears L1 and L2. For comparison, data of a configuration with the clean underbody, but without landing gear, are added. The drag curves reveal that the configurations with faired skid landing gears generate about 25% less drag with respect to the baseline variant at 0° and small negative AOAs. The L1 variant develops slightly higher drag than the L2 variant at positive AOA. Both modifications lead to a drag level much closer to that of the configuration without landing gear than to that of the baseline configuration. From -10° AOA to 0° AOA all curves show a decreasing drag coefficient. The baseline configuration has its minimum at 0° AOA, while the modified variants show a minimum around + 5° AOA (also see [10]).

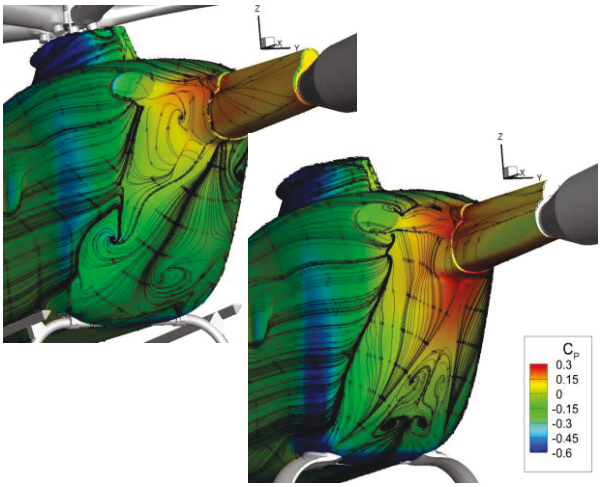

Fig.13. Pressure coefficient distribution on rear fuselage and backdoor region and surface streamlines based on URANS-SST; Re = 1 x 10^6, Ma_∞ = 0.116, AOA = 0°, AOS = 0°, baseline L0 (left) and modification L1 (right)

The analysis of the experimental data is supported by the results of the URANS-SST simulations. Fig. 13 presents the surface pressure distribution (pressure coefficient C_p) and superimposed surface streamlines. For the baseline configuration, the separating shear layers in the aft-body outboard regions do not roll up into a concentrated upsweep vortex along each side. Instead, vortex pairs are formed in the lower and upper aft-body area, indicated by the converging streamlines at the side edge regions (Fig. 13 left). In contrast, the aft-body streamline pattern of the configuration L1 (retrofit variant) indicates the evolution of a strong upsweep vortex (Fig. 13 right). The associated separation line extends nearly over the complete side edge area. Hence, the flow topology in the aft-body region is changed from an eddy-type wake flow for the baseline case to a wake flow dominated by a pronounced upsweep vortex pair. The surface pressure distribution substantiates the positive effect of the faired skid landing gear on interference drag. The backdoor region of increased pressure is significantly enlarged.

Performing drag reduction by shape optimization implies the need to prove its effects on the other aerodynamic coefficients. Analogous to the diagram in Fig. 12, Fig.14 shows the experimentally obtained lift coefficients as a function of AOA for the particular configurations. The characteristics of the lift curves confirm the results of the flowfield analysis. The streamlining of the skid landing gear's crossbeams causes larger regions of attached flow leading to an upwards deflection at the fuselage upsweep. In consequence, this flow pattern generates more downforce around 0° and negative AOAs. This effect is superimposed by the potentially lift- or downforce-generating airfoil-shaped components of the skid landing gear.

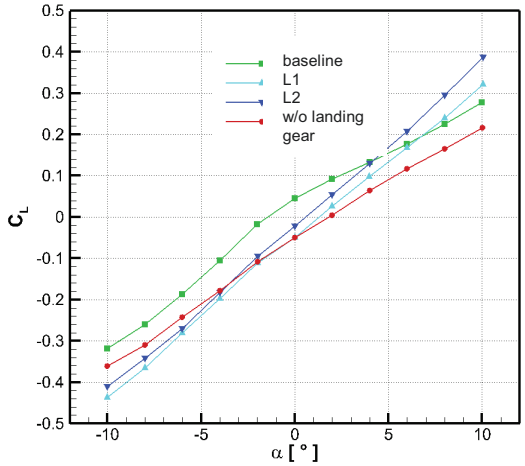

Fig.14. Lift coefficient vs AOA , AOS = 0°, Re = 1x10^6

As an important aerodynamic coefficient for the longitudinal stability, the pitching moment coefficient is shown in Fig.15. The modified variants, especially L2, generate a slightly higher pitching moment coefficient than the baseline variant at 0° AOA. As in the discussion of the lift coefficients already stated, the angle of incidence of the airfoil-shaped fairings must be taken into consideration as a likely source of changes in the aerodynamic coefficients. A further refinement of their design, notably an adaption of the angle of incidence, seems to be a suitable corrective measure.

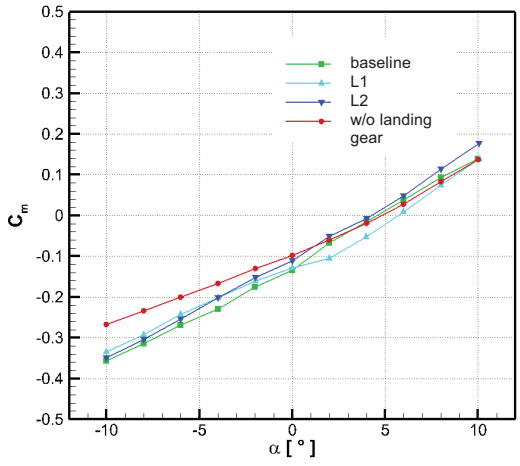

Fig.15. Pitching moment coefficient vs AOA , AOS = 0°, Re = 1x10^6

As a result of the skid landing gear modification campaign, the configuration with retrofit skid landing gear L1 is chosen as the reference configuration for the further modification steps. Modification L2 offers only minor advantages, which do not compensate for the effort of a necessary structural redesign. The modification of the fuselage aft-body with flow control elements, as well as the optimization of the mast fairing and the rotor hub, are carried out using this configuration (see Fig.9).

3.3. Strakes and Vortex Generators

In order to investigate the drag reducing potential of passive flow control devices at the aft-body, vortex generators (VGs) and strakes are tested. These devices are intended to decrease the portion of separated flow around the strong curvature of the backdoor.

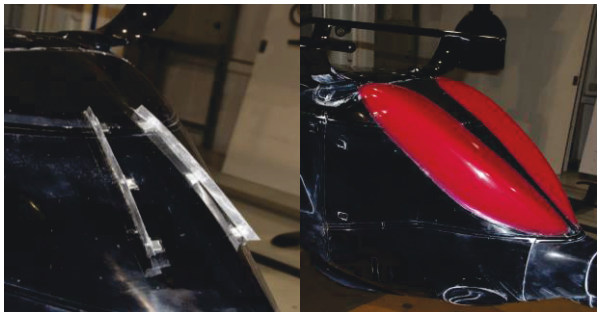

Fig.15. Strakes, S1 (left) and S2 (right)

The following flow control elements are chosen for intensive testing:

- Straight strakes S1
- Contoured strakes S2
- Vortex generators VGs

Regarding position and size, the S1 type strakes and the vortex generators evolved from parameter studies performed during preliminary wind tunnel tests. The S1 strakes are formed by flat plates of constant width, which are mounted perpendicular to the backdoor surface. Two of these elements are positioned symmetrically to the centerline, inboard of the backdoor's strong surface curvature. The contoured strakes S2 (Fig 15 right) are an outcome of an automated shape optimization process performed by the German Aerospace Center (DLR) and Airbus Helicopters using DLR's TAU code with a gradient decent approach (see [6]). The vortex generators (Fig.16) are designed to create pairs of counter rotating small scale streamwise vortices feeding energy to the boundary layer. The design of the vortex generators resulted from numerical flow simulations performed with the baseline configuration. The height of the vortex generators corresponds to the numerically obtained boundary layer thickness δ. An appropriate vortex generator length is approximately 3.5 δ and the inclination relative to the incoming flow is set to ±15°. The spacing between neighboring pairs of vortex generators (see [11]), allows a maximum of 5 vortex generator pairs in the region of interest. The position and number of these pairs of vortex generators had been determined by pretests in the wind tunnel. A systematic variation of the position, extension, and height of the straight strakes (S1), as well as the position and number of the vortex generators, has been carried out. This results in the most effective variants:

- S1 combined with two vortex generator pairs
- S2 combined with two vortex generator pairs.

The optimum positions of these devices on the fuselage are shown in Figures 15 and 16.

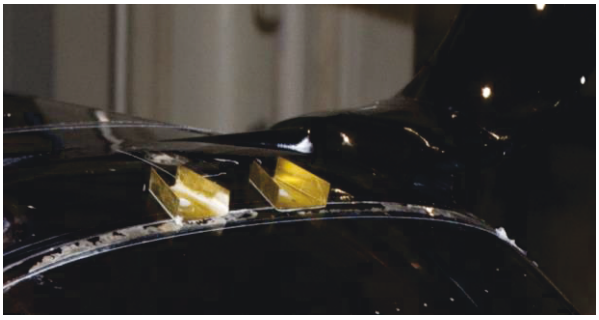

Fig.16. Belly mounted vortex generator pair

The strake and vortex generator related effects on the flowfield are analyzed using PIV velocity data. A comparison of the mean axial velocity in the wake of the two modified configurations with flow control devices is given in Fig.17. As a reference, the data of the unmodified configuration is added (Fig.17 top).

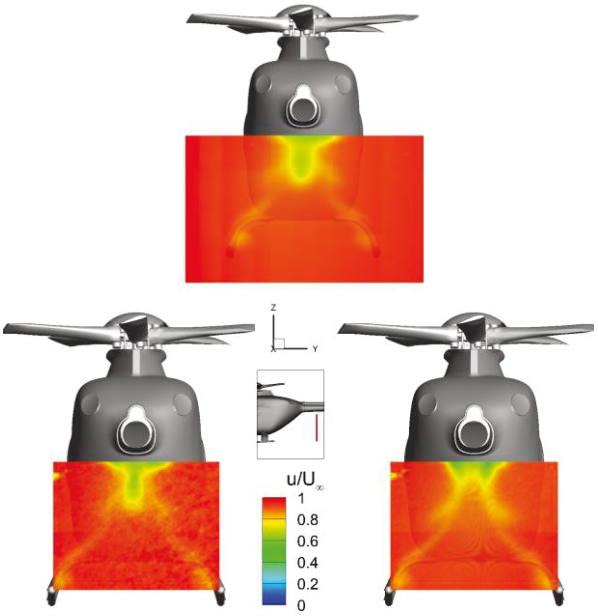

Fig.17. Mean axial velocity distribution: u/U_∞, AOA, AOS = 0°, configuration without flow control (top), configuration with S1 and VGs (bottom left) and configuration with S2 and VGs (bottom right), PIV result, Re = $1x10^6$

A positive effect of the combination of S1 type strakes with vortex generators is revealed by a further reduction of the axial velocity deficit located in the wake of the backdoor section (Fig.17 bottom left). The combination

of S2 type strakes with vortex generators shows a distinct reduction of the axial flow velocity deficit in the wake of the backdoor below the tail boom, indicating that the flow follows the fuselage upsweep until close to the tail boom (Fig.17 bottom right). The related drag polars of the three examined configurations are shown in Fig. 18. The flow control measures lead to a drag saving of about 4% with respect to the unmodified variant at 0° AOA. For the combination of S1 type strakes with vortex generators this drag saving can be achieved for almost the whole investigated AOA range. The drag polar of the combination of S2 type strakes with vortex generators shows a similar behavior, but slightly smaller drag reduction at negative (<-6°) AOAs.

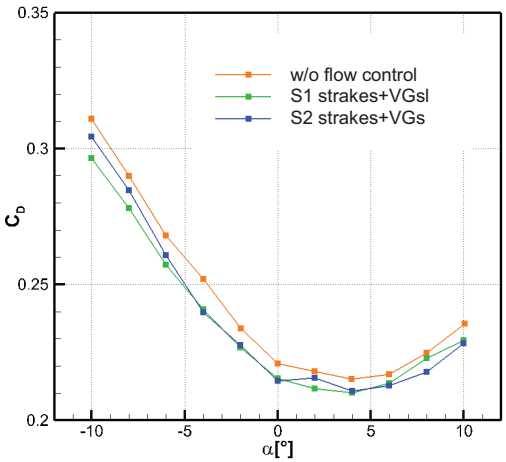

Fig.18. Drag coefficient vs AOA , AOS = 0°, Re = 1x10^6,

The effects of the flow control measures on the lift coefficient are depicted in Fig 19. Evidently, the combination of S1 strakes with vortex generators has no significant influence on the lift coefficient, while the combination of S2 type strakes with vortex generators generates less lift or an additional downforce over the whole AOA range.

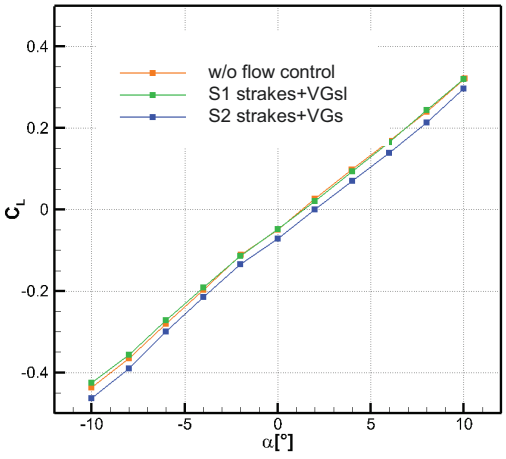

Fig.19. Lift coefficient vs AOA, AOS = 0°, Re = 1x10^6

The pitching moment coefficient as a function of AOA is shown in Fig.20. Noteworthy is the decrease of the pitching moment caused by the flow control devices around AOA = 0°, i.e. flow conditions close to that of a trimmed fast forward flight. The changes in the lift and pitching moment coefficients originate from the reduced flow separation at the aft-body. Again, the flow control devices can have influence on the flow conditions at the airfoil-shaped crossbeam fairings.

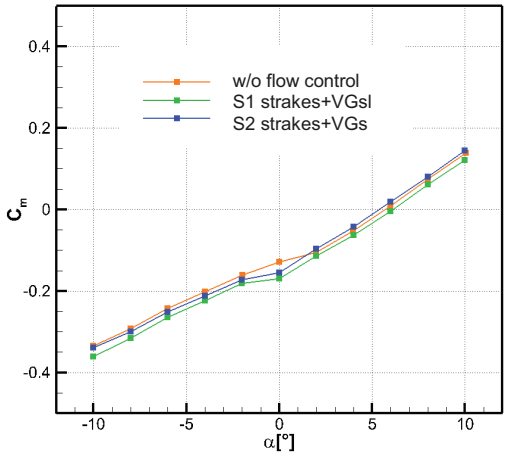

Fig.20. Pitching moment coefficient vs AOA, AOS = 0°, Re = 1x10^6

3.4. Mast Fairing Modification

In the final phase of ADHeRo, the mast fairing and rotor hub are subject to modifications with the purpose of drag reduction and improving the flowfield in the wake of the rotor. The paper presents results obtained with two mast fairing modifications M1 and M2. Fig. 21 shows the geometries of the baseline mast fairing M0 and the modified variants M1 and M2.

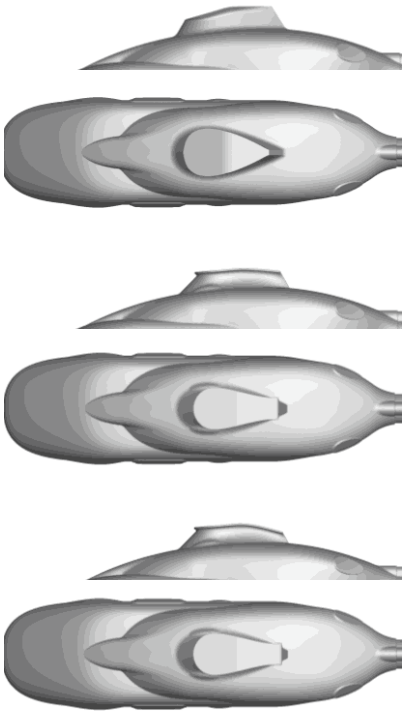

Fig.21. Mast fairing variants (from top to bottom), M0 (baseline variant), modification M1, and modification M2

Fig.22 shows the surface pressure distribution on the upper fuselage downstream of the mast fairings M0 (left) and M1 (right). Plotted is the pressure coefficient Cp interpolated on the model's surface by means of a Kriging function. The red dots mark the positions of the pressure taps with near-surface mounted sensors, and the black dots mark the taps connected to the pressure scanning system. For creating the interpolated pressure distribution, the time series taken with the transient sensors are averaged and combined with the steady pressure data taken from the pressure scanning system.

Analyzing the results of the pressure measurement, does not reveal any significant change in the surface pressure distribution downstream of the mast fairing. The modified mast fairing M2 gives an almost identical result.

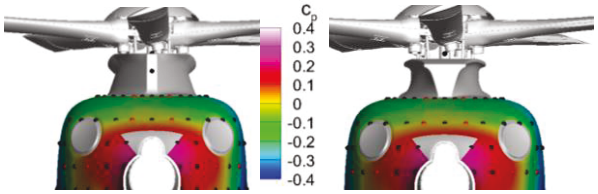

Fig.22. Surface pressure distribution (C_p), configuration with mast fairing M0 (left), with mast fairing M1 (right), Re = 1x10^6

Nevertheless, the measurement of forces and moments reveal a drag reducing effect of both modified mast fairings. The potential of the particular mast fairing modifications can be seen in Fig.23. In order to examine the sole effect of the incoming flow on the mast fairing modifications, results from experiments without rotor head are presented.

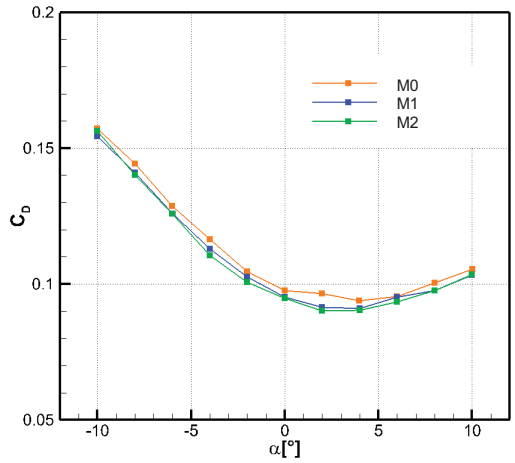

Fig.23. Drag coefficient vs AOA, AOS = 0°, Re = 1x10^6

Both mast fairing modifications lead to a slight drag reduction within the investigated AOA range. Around 0° AOA the benefit accounts for 1-2 % with respect to the baseline variant. The characteristics of the drag curves of the two modified variants feature an almost identical behavior.

The AOA-polars of the lift and pitching moment coefficients (see Figures 24 and 25) differ only for positive AOAs. The modified mast fairings cause a higher lift and pitching moment than the baseline mast fairing. Considering the typical flow conditions of a fast forward flight with a slightly negative AOA, this change in lift and pitching moment is not particularly relevant.

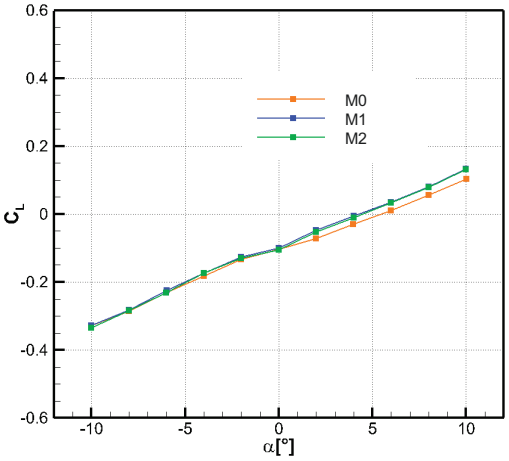

Fig.24. Lift coefficient vs AOA, AOS = 0°, Re = 1x10^6

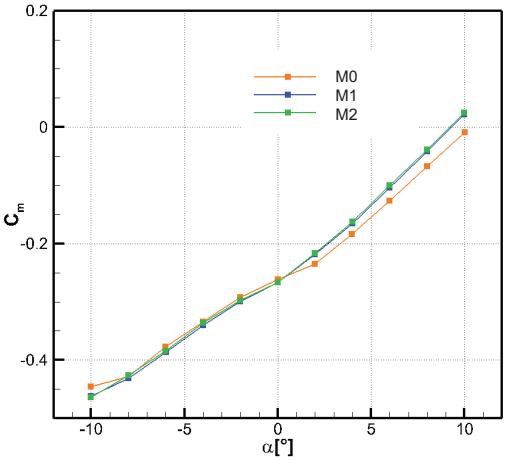

Fig.25 Pitching moment coefficient vs AOA, AOS = 0°, Re = 1x10^6

4. SYNTHESIS

Summing up the achievements of the drag optimization efforts up to this point, the drag reduction related to the particular modification steps is presented in Fig.26. Here, the chosen reference is an actual TEL-class helicopter including tail, stabilizers, upper deck, excrescences, and all other relevant sources of drag. The experimentally determined drag savings attained during the shape optimization process are scaled up accordingly. The data refer to flow conditions with AOA and AOS = 0°, approximately corresponding to the trimmed fast forward flight conditions.

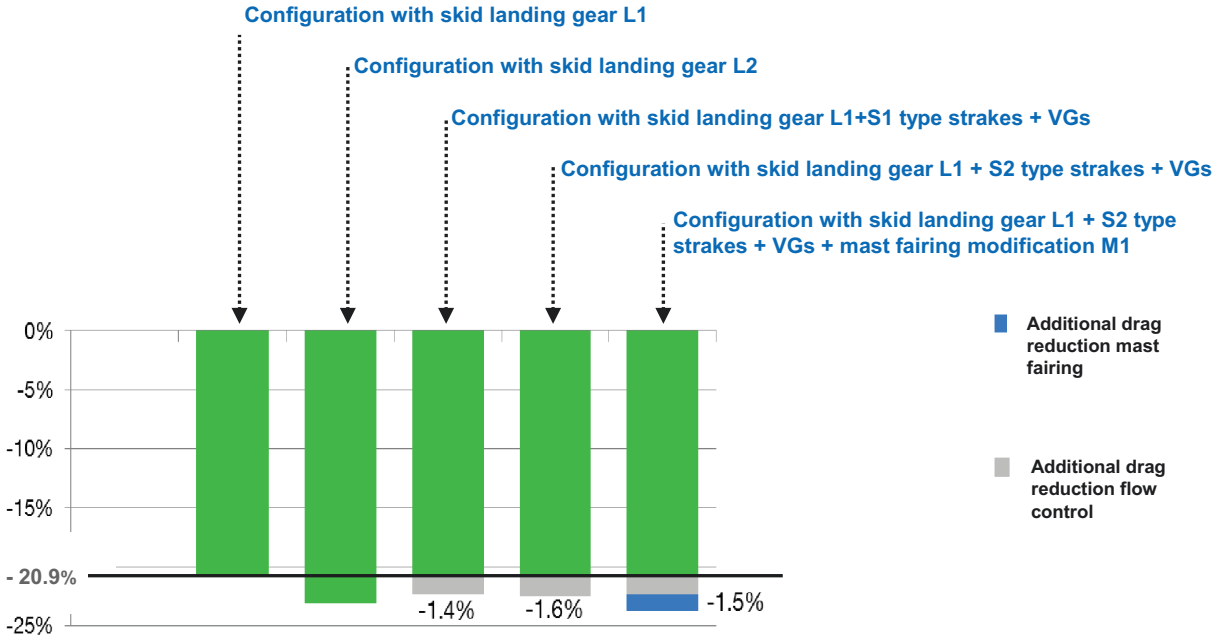

Fig.26. Achieved drag savings, scaled up to an actual TEL-class helicopter, AOA = 0°, AOS = 0°

The results of the investigations demonstrate that a drag reduction of up to 22.5% is possible by means of retrofit measures, including skid landing gear L1, contoured strakes S2, and vortex generators. With the simplified S1 type strakes still 22.3% drag reduction can be achieved. The modified mast fairing M1 renders an additional 1.5% drag reduction possible. During a final refinement process, the results of the rotor hub optimization are introduced into the design, offering additional benefits with respect to drag reduction.

5. CONCLUSIONS

Within the framework of the Clean Sky Joint Technology Initiative, the Green Rotorcraft Consortium subproject ADHeRo 'Aerodynamic Design Optimization of a Helicopter Fuselage including a Rotating Rotor Head' has been established to improve the aerodynamic efficiency of twin engine light class utility helicopters focusing mainly on drag reduction means. This paper presents results for skid landing gear modifications, aft-body flow control devices, and mast fairing modifications. The data are based on wind tunnel experiments and complementary fluid dynamics simulations which confirm the drag reduction potentials for faired skid landing gears and manipulation of the backdoor flow. In comparison to the reference configuration, considerable drag savings have been achieved, namely 20.9% and 23.1%, respectively, due to the faired skid landing gears which include a retrofit and a progressive variant. Employing the flow control elements, a further drag reduction of 1.4% in the case of the simplified strakes combined with vortex generators, and 1.6% in the case of the contoured strakes combined with vortex generators, can be attained. The vortex generators are located at the fuselage belly ahead of the strong backdoor upsweep. Thus, the investigated configurations exceed the expected drag benefits with 22.5% in the aggregate for easily retrofittable solutions. The technology readiness level of the configuration modifications is such that the proposed configuration modifications could be realized shortly after the end of the project. Thus, ADHeRo is making an important contribution to the reduction of the environmental impact of lightweight utility helicopters. The added benefit of reduced operational costs through reduced fuel consumption will help to fasten the process of applying the drag reduction means.

Acknowledgement

The research leading to these results received funding from the European Community's Seventh Framework Program (FP/2007-2013) for the Clean Sky Joint Technology Initiative under grant agreement number 270563. The authors also would like to express their gratitude to the project partner Airbus Helicopters Deutschland GmbH for fruitful cooperation and support. Furthermore, special thanks are addressed to ANSYS® for providing the flow simulation software.

Literature

[1] Clean Sky JTI, Green Rotorcraft; http://www.cleansky.eu, [cited August, 2014]

[2] Kneisch, T, Krauss, R, D'Alascio, A, and Schimke, D. Optimised Rotor Head Design for an Economic Helicopter. Proc. 37th European Rotorcraft Forum, Gallarate, Italy, 2011.

[3] Le Chuiton, F, Kneisch, T, Schneider, S, and Krämer, Ph. Industrial validation of numerical aerodynamics about rotor heads: towards a design optimisation at Eurocopter*", Proc. 35th European Rotorcraft Forum*, Hamburg, Germany, September 22 - 25, 2009.

[4] Wagner, S N. Problems of Estimating the Drag of a Helicopter, *AGARD Conference Proceedings No. 124*, April, 1973.

[5] Grawunder, M, Reß, R, and Breitsamter, C. Optimized Skid-Landing-Gears For Twin-Enegine-Light Utility Helicopter. *Proc. 39th European Rotorcraft Forum, ERF–2013–093*, Moscow, Russia, Sept. 3-6, 2013, pp. 093.1– 093.14.

[6] Zhang, Q, Garavello, A, D'Alascio, A, Schimke, D. Advanced CFD-based Optimization Methods Applied to the Industrial Design Process of Airframe Components at Airbus Helicopters, *Proc. AHS 70th Annual Forum*, Montréal, Québec, Canada, May 20–22, 2014, pp. 1-13.

[7] Grawunder, M, Reß, R, Breitsamter, C, and Adams, N A. Flow Characteristics of a Helicopter Fuselage Configuration Including a Rotating Rotor Head. *ICAS Proc., 28th Congress of the International Council of the Aeronautical Sciences, ICAS–2012–2.7.3*, Brisbane, Australia, Sept. 23-28, 2012, pp. 273.1– 273.14.

[8] ANSYS, Inc., CFX – Solver Theory Guide Release 14.5, 2012.

[9] Grawunder, M, Reß, R, Stein, V, Breitsamter, C and Adams N A. Flow Simulation of a Five Bladed Rotor Head. *New Results in Numerical and Experimental Fluid Mechanics IX, NNFM,* Vol. 124, 2010, pp. 235-243.

[10] Reß, R, Grawunder, M, Breitsamter, C. Aerodynamic Analysis of a Helicopter Fuselage with Rotating Rotor Head, *Proc. 5th European Conference for Aeronautics and Space Sciences, (EUCASS)*, Munich, Germany, July 1-5, 2014

[11] Gad-el-Hak, M. *Flow Control – Passive, Active, and Reactive Flow Management*, Cambridge University Press, 2000.